AGU PUBLICATIONS

JGR

Journal of Geophysical Research: Space Physics

RESEARCH ARTICLE
10.1002/2013JA019491

Key Points:
- Long-lasting characteristic of wind and TEC anomalies in the MLT and ionosphere
- Local-time migration of TEC and vertical drift anomalies during SSW
- Amplification of MLT winds and TEC oscillations during SSW

Correspondence to:
O. F. Jonah,
davjayus@yahoo.com

Citation:
Jonah, O. F., E. R. de Paula, E. A. Kherani, S. L. G. Dutra, and R. R. Paes (2014), Atmospheric and ionospheric response to sudden stratospheric warming of January 2013, *J. Geophys. Res. Space Physics*, *119*, 4973–4980, doi:10.1002/2013JA019491.

Received 2 OCT 2013
Accepted 18 MAY 2014
Accepted article online 28 MAY 2014
Published online 13 JUN 2014
Corrected 7 JUL 2014

This article was corrected on 7 JUL 2014. See the end of the full text for details.

Atmospheric and ionospheric response to sudden stratospheric warming of January 2013

O. F. Jonah[1], E. R. de Paula[1], E. A. Kherani[1], S. L. G. Dutra[1], and R. R. Paes[1]

[1]National Institute for Space Research, São José Dos Campos, Brazil

Abstract In this work, we examine the atmospheric and ionospheric responses to the January 2013 sudden stratospheric warming (SSW) event. To examine the atmospheric and ionospheric behavior during this event, three main parameters are used (1) Total Electron Content (TEC) collected from the International Global Positioning System and from the Brazilian Network of Continuous Monitoring stations, (2) daytime E × B vertical drift derived from the magnetometers located at the equatorial station Alta Floresta (9.9°S, 55.9°W, dip latitude 1.96°) and an off-equatorial station Cuiaba (15.3°S, 56.0°W, dip latitude 7.10°), both in the Brazilian sector, (3) the mesosphere and lower thermosphere (MLT) meridional and zonal wind components measured by the Meteor Radar located at the southern midlatitude Santa Maria (29.4°S, 53.3°W, dip latitude 17.8°). We identify the anomalous variation in E × B drift based on later local-time migration of peak value with SSW days. A novel feature of the present study is the identification of the similar migration pattern in the TEC anomaly, in spite that the simultaneous solar flux increases during the SSW event. Other novel features are the amplification of the 13–16 day period in the TEC anomaly during the SSW days and simultaneous amplification of this period in the meridional and zonal wind components in the MLT region, as far as 30°S. These aspects reveal the presence of coupled atmosphere-ionosphere dynamics during the SSW event and the amplification of the lunar and/or solar tidal component, a characteristic which is recently reported from the electrojet current measurements.

1. Introduction

There are many important parameters that can be used to study the ionospheric variabilities. One of them is the total electron content (TEC). The TEC is responsible for time delay which produces range errors in the GPS radio signal of a satellite to ground radio communication that can seriously affect space weather forecast [*Rastogi and Klobuchar*, 1990]. Another important parameter for plasma description is the behavior of E × B vertical drift which plays a crucial role in the dynamics of the low-latitude ionosphere variation. The largest ionospheric perturbations have been attributed to geomagnetic activity. However, during geomagnetic quiet times, the ionospheric perturbation could also result from meteorological processes such as planetary waves, gravity waves, tides, etc.

Large-scale electrodynamics and plasma density variation of the ionized layer have been recently associated with SSW events which have been a subject of intensive study [e.g., *Goncharenko and Zhang*, 2008; *Goncharenko et al.*, 2010; *Liu et al.*, 2010 and *Fejer et al.*, 2011]. A SSW event is characterized by a sudden breakdown of the stratospheric polar vortex caused by dynamical forcing of upward propagating planetary waves from lower atmospheric layers. The nonlinear interaction between the zonal mean flow and the growth of vertically propagating planetary waves leads to stratospheric temperature increase by several tens of degrees initiating the anomaly process. During this period the eastward zonal wind flow could abruptly slow down (minor warming) or turn westward, i.e., reverses direction (major warming) consequently causing the breakdown of the polar vortex. These mechanisms are known to be the major driver of anomalies in the middle atmosphere, which is referred to as SSW. The SSW was first observed in 1950s (e.g., *Scherhag* [1952] and later by *Chau et al.* [2012]), and since then many studies have revealed the coupling between stratosphere and ionosphere [e.g., *Goncharenko and Zhang*, 2008 and *Chau et al.*, 2010]. At low-middle latitudes, SSW is associated with warming in the lower thermosphere and cooling in the upper thermosphere, with both features exhibiting semidiurnal behavior [*Goncharenko and Zhang*, 2008 and *Pedatella and Liu*, 2013]. Although the physics behind atmospheric tides and planetary waves influences over the ionosphere are generally well understood, it is not still certain about the processes responsible for generating ionospheric variability in connection with SSWs. Evidence from *Goncharenko and Zhang* [2008] shows a

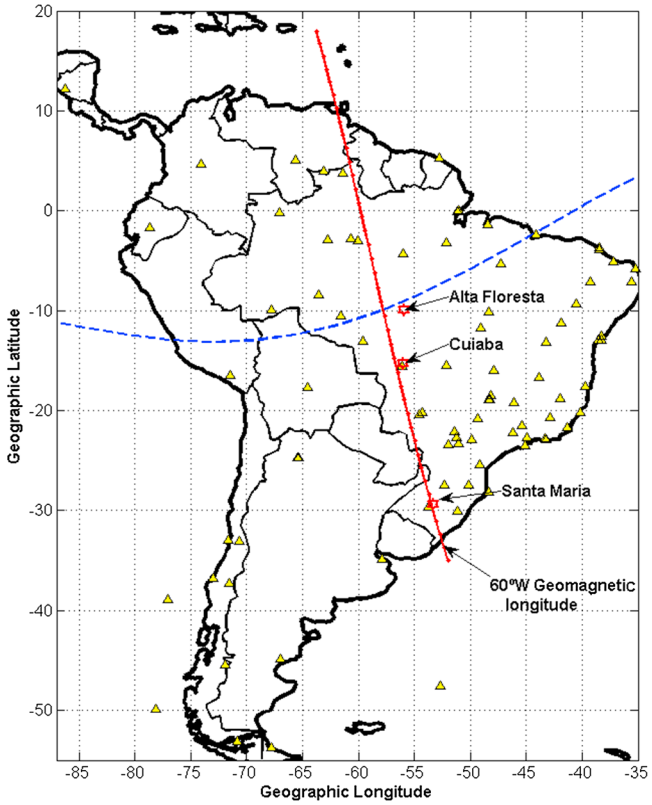

Figure 1. GPS receiver network over South America using International Global Positioning System and Brazilian Institute of Geography and Statistics (IBGE) network. The blue dash line represents the geomagnetic equator while the red line represents the geomagnetic meridian of 60°W longitudes. The red stars representing Alta Floresta and Cuiaba are the equatorial and off-equatorial magnetometer stations which are used to derive the equatorial vertical drift. The red star representing Santa Maria is the meteor radar site that is used to obtain the wind data.

primarily semidiurnal modulation of the ionosphere during the 2008 SSW, and they suggested that enhanced planetary wave activity associated with SSWs plays an important role in producing the ionospheric perturbations. It is clear from the conclusion of *Fejer et al.* [2011] and *Park et al.* [2012] that SSW event is associated with an amplification of the lunar tide that modulates the low-latitude and midlatitude ionosphere. *Liu et al.* [2010] proposed that the observed semidiurnal perturbations in the ionosphere are due to the nonlinear interaction between migrating tides and planetary waves. However, significant changes in the tidal winds were found to occur in the low-latitude *E* region where electric fields are generated by the dynamo mechanisms, resulting in modulation and enhancement of the vertical drift velocity and electron densities in the ionosphere. According to *Pancheva et al.* [2009] intensified nonmigrating tides linked with the nonlinear interaction between planetary waves and migrating tides could also be observed in the stratosphere and lower mesosphere temperatures during the 2003/2004 SSW.

In this work, we study a recent SSW event that occurred during January 2013. We present the behavior of the atmosphere and low-latitude ionosphere over the Brazilian region, based on the measurements of the TEC distribution along 60°W of magnetic longitude, vertical drift of the equatorial ionosphere and mesosphere wind under equatorial ionization anomaly (EIA) crest. These multiinstrument observations may help us to better understand the simultaneous presence of varieties of tidal waves, namely, semidiurnal solar and lunar tides, in both atmospheric and ionospheric observables. In section 2, we present the methodology adopted to estimate the TEC and vertical drift. In section 4, the characteristics of January 2013 SSW event are presented. In section 5, the results are presented and discussed.

2. Methodology

Over Brazil, fairly dense dual-frequency GPS network enable us to measure the TEC with reasonably high spatial resolution [*Muella et al.*, 2010]. In order to obtain the vertical TEC from the measured TEC, we employ the Nagoya model [*Otsuka et al.*, 2002]. The method has been validated using International Reference Ionosphere model and compared with the incoherent-scatter middle and upper atmospheric radar (MU radar) observation. It was found that the Nagoya method underestimated TEC by less than 3 TECU (total electron content unit, 1 TECU = 10^{16} el m^{-2}) and was 2 TECU larger than the MU radar TEC on average. This difference can be attributed to the plamasphere electron content along the GPS ray path [*Otsuka et al.*, 2002]. TEC data were collected from a wide range of geomagnetic latitudes (±20°) and along the geomagnetic meridian of 60°W corresponding to the geographic longitudes located between 52°W and 60°W as shown in Figure 1.

Simultaneously, the magnetometer network over Brazil enable us to measure the vertical E × B ion plasma drift of the ionosphere based on methodology described by *Anderson and Anghel* [2004]. The strength of the daytime equatorial electrojet, which is proportional to the vertical equatorial plasma drift, could be measured using two magnetometers, one located on the magnetic equator (Alta Floresta, 9.9°S, 55.9°W, dip latitude 1.96°) and the other displaced by 6–9° away from the equator (Cuiaba, 15.3°S, 56.0°W, dip latitude 7.10°) [*Rastogi and Klobuchar*, 1990].

The MLT wind data obtained using meteor radar at Santa Maria (29.4°S, 53.3°W, dip latitude 17.8°) are used to infer the meridional and zonal wind. The meteor radar system is an All-Sky Interferometric Meteor Radar (SKiYMET) type with operating frequency of 35.24 MHz. It utilizes 13 pulse width, with a peak power of 12 kW and pulse repetition frequency of 2 kHz. Due to practical limitations, the received data are obtained within the zenith angle range 17–70°, since at lower zenith angle ($<$15°) radial velocity errors are excessive and at higher zenith angle ($>$70°) the signal gets contaminated with ground clutter and airplane echoes. The radar detects about 5000 meteor echoes per day for which it estimates angular position, range, and radial velocity. Details about the radar can be found in *Hocking et al.* [2001]. The received horizontal wind data are analyzed at a range resolution of 3 km and time resolution of 1 h in the altitude range 81–99 km.

3. The 2013 SSW Event

Figure 2 shows the summary of stratospheric, solar, and geomagnetic conditions for the winter solstice in the Northern Hemisphere of 2013, which was one of largest and strongest SSW events in recent history. Stratospheric data were collected from the National Centre for Environmental Prediction, geomagnetic data were collected from http://wdc.kugi.kyoto-u.ac.jp/ website, and the solar flux data were collected from http://omniweb.gsfc.nasa.gov/form/dx1 website. The red lines, common to the first to fifth panels, represent the data, respectively, from 1985 to 2013.

Figure 2 (first and second panels) represents the stratospheric temperature at 90°N and mean of stratospheric temperature at 90–60°N both at 10 hPa (~32 km). There is a sharp increase in both cases by more than 50 K (from day 4 to day 6, January 2013). We observed two temperature peaks of the 90° temperature, the first one occurred on 6 January and second peak was observed on 12 January. Figure 2 (third panel) shows the zonal mean wind at 60°N, which reversed from eastward to westward indicating a major warming. Figure 2 (fourth panel) indicates the planetary wave number 1 activity at 60°N which exceeds the long-term mean level by a factor of ~2 (during days 15–24 December 2012) that could be responsible for the first temperature increase. The sudden increase in planetary wave number 2 shown in Figure 2 (fifth panel) which exceeds the long-term mean level by a factor of ~3 (during days 6–8 January 2013) could be a main factor for the second increase in the stratosphere temperature. Figure 2 (sixth and seventh panels) presents indices for solar flux and geomagnetic activity. Although this period was geomagnetically quiet, it was marked by a strong increase in solar flux that was a part of 27 day solar variation and coincided with stratospheric temperature increase.

4. Results

In Figure 3, observed TEC and magnetometer-deduced E × B drift of the ionosphere during 3 months covering SSW days are shown. This TEC is from 60°W and ±20° latitudinal averaged. It is understood that the averaging is affected by the EIA dynamics which is highly variable in nature both in space and time that may be caused by both SSW forcing and non-SSW forcing. For this reason, we present both TEC and ΔTEC averaged characteristic. This will ensure that any common characteristic in both TEC and ΔTEC during SSW period should be associated with the SSW forcing and will eliminate non-SSW forcing effects arising from the averaging. In Figure 3 (top row), TEC and TEC anomaly (ΔTEC) are plotted, respectively. In Figure 3, (middle row), drift and drift anomaly (ΔV) are plotted, respectively. In Figure 3 (bottom row), the drifts are plotted for few selected SSW days (hereby called active days) and few days of suppressed vertical plasma drifts as compared with the 3 month mean, respectively. The anomalies given by $\Delta TEC = TEC - TEC_{av}$ and $\Delta V = V - V_{av}$, where the average values are obtained by averaging the TEC and V values. Data during these 3 months are classified based on the lunar phase. We then estimate the averages (TEC_{av}, V_{av}) during each phase. Subsequently, we estimate the anomalies, ΔTEC and ΔV, for each lunar phase, i.e., the difference between each data set and the corresponding average of that lunar phase for which the data set belongs. The

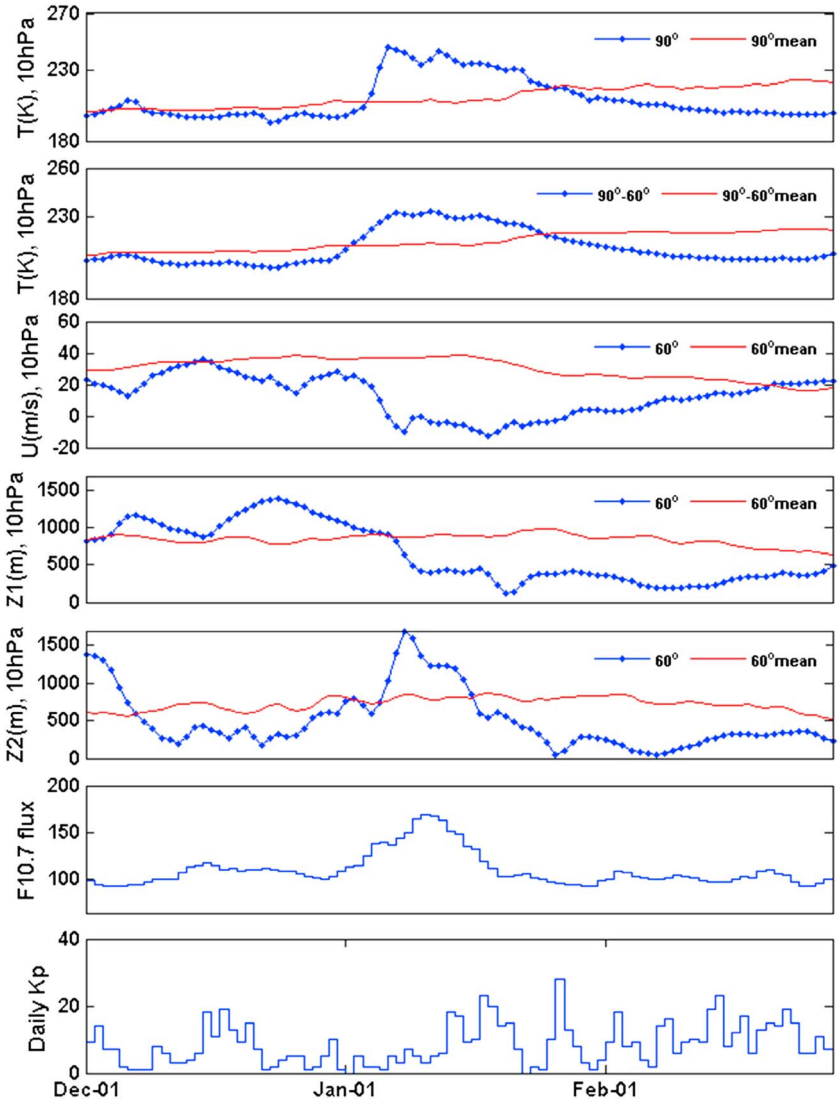

Figure 2. Summary of stratospheric, solar, and geomagnetic conditions for the 2013 SSW events. (top to bottom) Stratospheric temperatures at 90°N, stratospheric temperature at 60°N, zonal mean wind at 60°N, planetary wave 1 at 60°N, and planetary wave 2 at 60°N. $F_{10.7}$ flux and daily *Kp* index. The red line indicates historical mean of stratospheric parameters.

gaps in plasma drift data were due to the lack of continuous magnetometer data. We have examined the anomalies by considering other two kinds of average: (i) the seasonally averaged (November–February) single value, (ii) the average value corresponding to the TEC and drift values on the day of previous lunar phase having same phase as the day for which anomaly is estimated. The anomalies obtained using these two approaches reveal similar characteristics of the anomalies as shown in Figure 3, though they are less pronounced under these two approaches.

We may note the following features: (1) the peak value of the TEC and corresponding anomaly progressively migrate to the later time, during active periods while such local-time migration is absent during quiet days, (2) the peak drift and corresponding anomaly also reveal local-time migration, similar to the TEC characteristics, and (3) compared to the lunar-phase averaged drift, the drifts during active period of 16–21 January are considerably higher, while drifts of 10 and 12 January exhibit lower values.

In Figure 4, the stratospheric temperature over high latitude (first panel), the meridional and zonal wind anomalies in the MLT region (second and third panels), and the TEC anomaly (fourth panel) are plotted, as

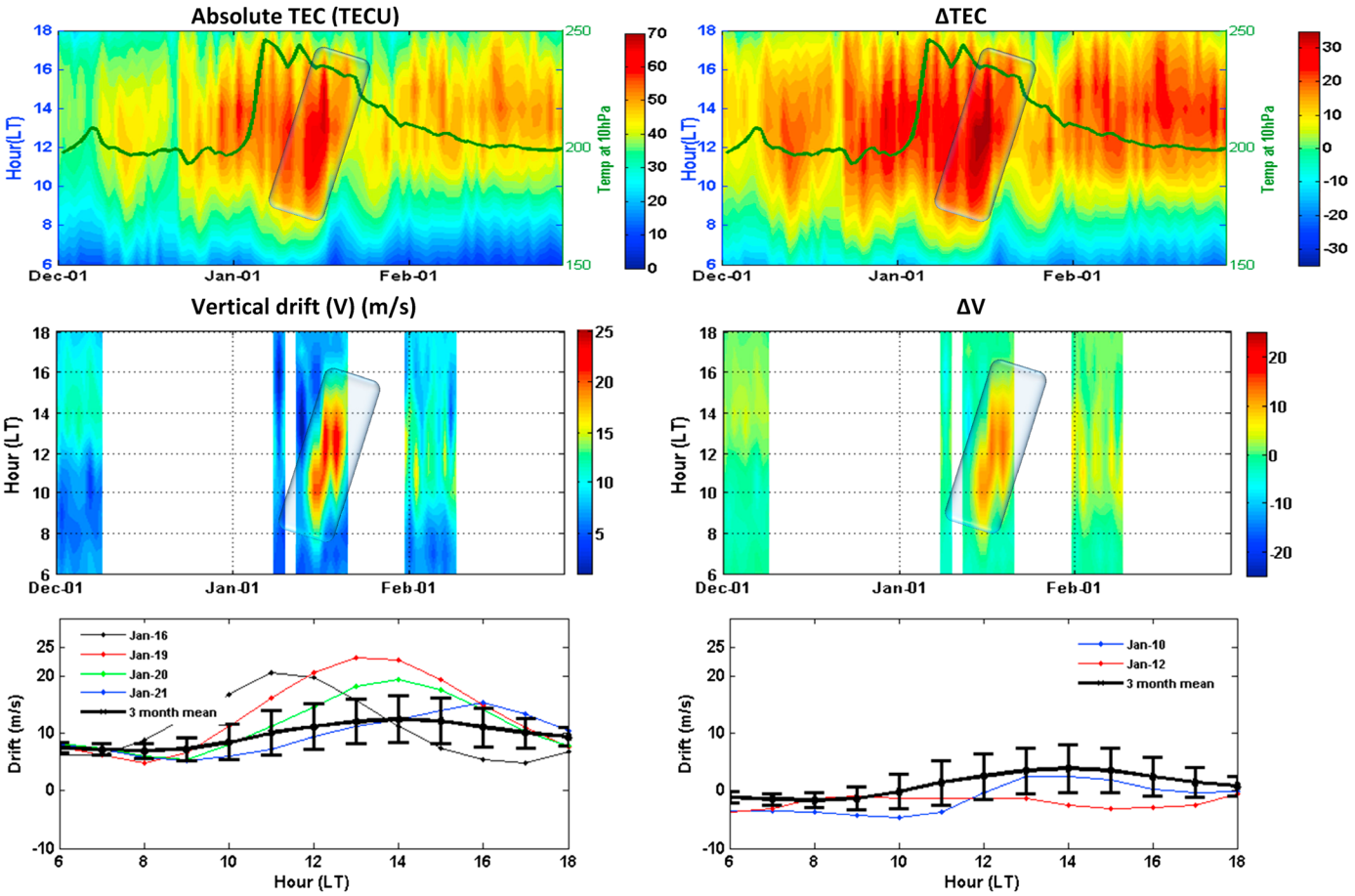

Figure 3. Three months TEC and 3 months magnetometer-deduced E × B drift of the ionosphere. (top row) TEC and TEC anomaly (ΔTEC), respectively. (middle row) Drift and drift anomaly (ΔV), respectively. (bottom row) The drifts for selected SSW days. The anomalies are represented by ΔTEC = TEC − TECav and ΔV = *V* − *V*av, where the average values are obtained by averaging the TEC and *V* values during each lunar phase.

blue curves, during December–February period. These anomalies correspond to the 12 local time, and TEC anomaly is the latitude averaged. Anomalies are obtained in the same way as described above in the context of Figure 3. Along with these anomalies, also plotted as green curves, are their corresponding band-pass filtered anomalies such that the period between 13 and 16 days are allowed to pass using Butterworth filter with order 2. The range of 13–16 days is chosen based on the wavelet spectra of time series of TEC and winds while the filter of order 2 is chosen to match the filtered times series with the wavelet spectra in this frequency band.

We may note the following characteristics: (4) the wind anomalies are considerably amplified during the active period (SSW period) as compared during the quiet period, (5) the filtered wind anomalies have spectral peak in 13–16 days period, which is considerably amplified during the active period, (6) the filtered TEC anomaly also reveals considerable amplification during the active period, (7) the filtered TEC anomaly stays amplified till February, i.e., it reveals a long-lasting amplification which is also the case for wind though not as pronounced as TEC anomaly.

5. Discussion

5.1. Local-Time-Migration Characteristics of the Ionospheric Drift and TEC (Figure 3)

The characteristics of ionospheric drift (noted as 2 and 3 from last section) are the same as those reported by the recent studies [*Chau et al.*, 2009; *Goncharenko et al.*, 2010; *Fejer et al.*, 2011]. As pointed out by *Goncharenko et al.* [2013], the local-time migration is the manifestation of the semidiurnal forcing of solar or

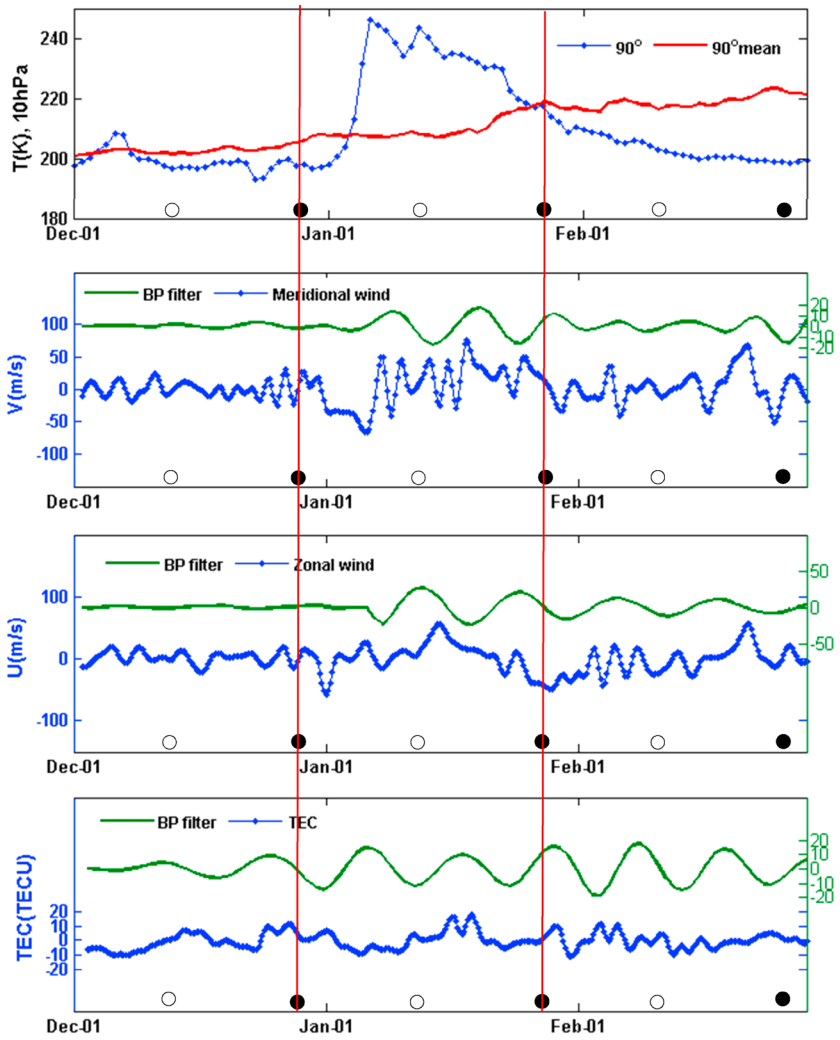

Figure 4. (first panel) The stratospheric temperature over high latitude, (second and third panels) the meridional (ΔV) and zonal (ΔU) wind anomalies in the MLT region, and the (fourth) TEC anomaly are plotted, as blue curves, during December to February period. Anomalies are obtained in same way as described in Figure 3. The green curves are the corresponding band-pass filtered anomalies such that the period between 13–16 days is allowed to pass using Butterworth filter. The new and full moons are indicated by white and black circle, respectively.

lunar origin. In the present study, the drifts are derived using magnetometer network and are based on *E* region current system. This suggests that a magnetometer network can efficiently capture similar ionospheric response from the *E* region current system as the direct *F* region drift measurements using incoherent-scatter radar. This drift is qualitatively similar to *Goncharenko et al.* [2013] during the same period but quantitatively different in spite that both studies use magnetometer measurements. The drifts over Brazilian and Peruvian sectors were found to be quantitatively different, and it is attributed to the four-wave structure [*Nogueira et al.*, 2013]. The quantitative difference between the present study and the study by *Goncharenko et al.* [2013] may possibly be arising owing to this four-wave structure.

In addition, the TEC characteristic noted as (1) is a novel feature that the present study brings out. The presence of similar local-time migration during active period in TEC and drift suggests that the TEC anomaly is a manifestation of the transport dynamics triggered by the E × B drift anomaly during the active period. It should be pointed out that the present study brings out this local-time-migration characteristic associated with the SSW though the solar flux is also increased substantially during the active period. The solar flux increase may drive transports such as the enhanced wind activity and enhanced ionization, both resulting in considerable

variation in the TEC and drift (V). In spite the presence of these variations arising from solar forcing, the local-time-migration characteristic is revealed in both TEC and *V* and their corresponding anomalies. This suggests that the semidiurnal forcing of SSW origin can be of similar magnitude as the forcing of solar flux origin.

It should be further pointed out that the similar behavior of drift anomaly in the present study at 60° magnetic meridian and the study by *Goncharenko et al.* [2013] at 70° magnetic meridian suggests that the forcing of SSW origin has considerable longer scale in the longitude and/or possibly has the dominant migrating tidal component than the nonmigrating component. Figures 3e and 3f, respectively, shows confirmation of *Goncharenko et al.* [2013] that the constructive (destructive) superposition of solar and lunar migrating tides can lead to daytime enhancement (very low) vertical drift.

5.2. Atmospheric-Ionospheric Coupling by Amplified 13–16 Days Period Wave Forcing (Figure 4)

The characteristic noted under (4) suggests that the MLT wind system is considerably modified during the active period. Moreover, (5) suggests that both meridional and zonal wind components have dominant spectra peak in period ~13–16 days, indicating the role of lunar and/or solar tidal forcing in the amplification of wind anomaly. *Park et al.* [2012] and *Fejer et al.* [2011] have reported the amplification of lunar tidal component in the *E* region current during several SSW events. In the present study, the similar amplification is noted in the MLT wind components suggesting that the lunar tidal component in the *E* region current is possibly driven by the wind anomaly during SSW events.

In addition, the characteristic noted under (6) suggests that the TEC anomaly, together with the *E* region current anomaly, is the manifestations of the atmospheric-ionospheric coupling dynamics where the MLT wind anomalies are considerably modified and amplified at period ~13–16 days, owing to the tides of either lunar or solar origin. Based on the works by *Fejer et al.* [2011] and *Park et al*. [2012], it may be suggested that the observed 13–16 days period in the present study has contribution from the lunar tidal forcing.

The characteristic (7) suggests that ionosphere reacts in different ways to different stages of SSW knowing that SSW 2013 was a long-lasting event. This long-lasting characteristic in the wind and TEC anomalies suggests the long-lasting forcing of SSW in the MLT region and ionosphere.

It should be emphasized that the MLT wind data presented in this study are from 30°S, and the presence of SSW effects as far as this latitude is noted. *Lima et al.* [2012] have studied few SSW events and presented the MLT wind from 7°S showing the wind anomaly associated with the SSW. The present study is farther away toward south, and the presence of wind anomalies suggests that SSW effects can reach as far as 30°S.

6. Conclusion

In this study, we present the observed characteristics of ionosphere and atmosphere over 60° magnetic meridian over Brazil during 2013 SSW event. These characteristics are associated with the TEC and $E \times B$ drift and MLT wind system as derived using GPS network, magnetometer network, and meteor radar, respectively. The data are presented in the form of absolute values and corresponding anomalies. The anomalies are defined as the absolute values minus an average value. The average value is estimated by averaging the daily absolute values during each lunar phase.

We identify the anomalous variation in $E \times B$ drift and corresponding anomaly, based on later local time migration of peak value with SSW days, as reported recently by *Goncharenko et al.* [2013], attributing it to the semidiurnal forcing of solar and/or lunar origin. This suggests that a magnetometer network can efficiently capture similar ionospheric response from the *E* region current system as the direct *F* region drift measurements using incoherent-scatter radar. A novel feature of the present study is the identification of the similar local-time-migration pattern in the TEC anomaly, in spite that the simultaneous solar flux increases during the SSW event acts as another forcing directly affecting the ionization and winds. This suggests that the semidiurnal forcing of SSW origin can be of similar magnitude as the forcing of solar flux origin.

Other novel features are the amplification of the 13–16 days period in the TEC anomaly during the SSW days and simultaneous amplification of these periods in the meridional and zonal wind components in the MLT region. These aspects reveal the presence of coupled atmosphere-ionosphere dynamics during the SSW event where the MLT wind anomaly is the driving source that is amplified owing to the forcing coming from

the lunar and/or solar tides. Moreover, the long-lasting characteristic in the wind and TEC anomalies suggest the long-lasting forcing of SSW in the MLT region and ionosphere. Lastly, this study also shows a strong evidence of large-scale anomalies in the Southern Hemisphere using the MLT wind data from ~30°S during SSW event of January 2013. The SSW effects extending to Southern Hemisphere as far as 30° are another novel feature of the presented study.

Acknowledgments

The authors are grateful to Bela G. Fejer and Anthea Coster for the valuable discussions and to Y. Otsuka for making the Nagoya model available. We also acknowledge Dr. Paulo Prado Batista for providing us with the meteor radar data. O.F. Jonah would like to thank CNPq under process 133429/2011-3 and E.A. Kherani to FAPESP under process 2011/21903-3. E.R. de Paula is grateful to AFOSR FA9550-10-1-0564 and CNPq 305684/2010-8 grants.

Alan Rodger thanks the reviewers for their assistance in evaluating this paper.

References

Anderson D., and A. Anghel (2004), Daytime vertical E×B drift velocities inferred from ground-based magnetometer observations at low latitudes, *Space Weather*, *2*, S11001, doi:10.1029/2004SW000095.

Chau, J. L., B. G. Fejer, and L. P. Goncharenko (2009), Quiet variability of equatorial E×B drifts during a stratospheric warming event, *J. Geophys. Res.*, *36*, L05101, doi:10.1029/2008GL036785.

Chau, J. L., N. A. Aponte, E. Cabassa, M. P. Sulzer, L. P. Goncharenko, and S. A. Gonzalez (2010), Quiet time ionospheric variability over Arecibo during sudden stratospheric warming events, *J. Geophys. Res.*, *115*, A00G06, doi:10.1029/2010JA015378.

Chau, J. L., L. P. Goncharenko, B. G. Fejer, and H. L. Liu (2012), Equatorial and low latitude ionospheric effects during sudden stratospheric warming events, *Space Sci. Rev.*, *168*, 385–417, doi:10.1007/s11214-011-9797-5.

Fejer, B. G., B. D. Tracy, M. E. Olson, and J. L. Chau (2011), Enhanced lunar semidiurnal equatorial vertical plasma drifts during sudden stratospheric warmings, *Geophys. Res. Lett.*, *38*, L21104, doi:10.1029/2011GL049788.

Goncharenko, L., and S. R. Zhang (2008), Ionospheric signatures of sudden stratospheric warming: Ion temperature at middle latitude, *Geophys. Res. Lett.*, *35*, L21103, doi:10.1029/2008GL035684.

Goncharenko, L. P., A. J. Coster, J. L. Chau, and C. E. Valladares (2010), Impact of sudden stratospheric warmings on equatorial ionization anomaly, *J. Geophys. Res.*, *115*, A00G07, doi:10.1029/2010JA015400.

Goncharenko, L., J. L. Chau, P. Condor, A. Coster, and L. Benkevitch (2013), Ionospheric effects of sudden stratospheric warming during moderate-to-high solar activity: Case study of January 2013, *Geophys. Res. Lett.*, *40*, 1–5, doi:10.1002/grl.50980.

Hocking, W. K., B. Fuller, and B. Vandepeer (2001), Real time determination of meteor related parameters utilizing modern digital technology, *J. Atmos. Sol. Terr. Phys.*, *63*, 155–169.

Lima, L. M., E. O. Alves, P. P. Batista, B. R. Clemesha, A. F. Medeiros, and R. A. Buriti (2012), Sudden stratospheric warming effects on the mesospheric tides and 2-day wave dynamics at 7°S, *J. Atmos. Sol. Terr. Phys.*, *78-79*, 99–107.

Liu, H.-L., W. Wang, A. D. Richmond, and R. G. Roble (2010), Ionospheric variability due to planetary waves and tides for solar minimum conditions, *J. Geophys. Res.*, *115*, A00G01, doi:10.1029/2009JA015188.

Muella, M. T. A. H., E. A. Kherani, E. R. de Paula, A. P. Cerruti, P. M. Kintner, I. J. Kantor, C. N. Mitchell, I. S. Batista, and M. A. Abdu (2010), Scintillation-producing Fresnel-scale irregularities associated with the regions of steepest TEC gradients adjacent to the equatorial ionization anomaly, *J. Geophys. Res.*, *115*, A03301, doi:10.1029/2009JA014788.

Nogueira, P. A. B., M. A. Abdu, J. R. Souza, G. J. Bailey, and I. S. Batista (2013), Longitudinal variation in Global Navigation Satellite Systems TEC and topside ion density over South American sector associated with the four-peaked wave structures, *J. Geophys. Res. Space Physics*, *118*, 1–14, doi:10.1002/2013JA019266.

Otsuka, Y., T. Ogawa, A. Saito, T. Tsugawa, S. Fukao, and S. A. Miyazaki (2002), New technique for mapping of total electron content using GPS network in Japan, *J. Earth Planets Space*, *54*, 63–70.

Pancheva, D., P. Mukhtarov, and B. Andonov (2009), Non-migrating tide activity related to the sudden stratospheric warming in the Arctic winter of 2003/2004, *Ann. Geophys.*, *27*, 975–987.

Park, J., H. Lühr, M. Kunze, B. G. Fejer, and W. K. Min (2012), Effect of sudden stratospheric warming on lunar tidal modulation of the equatorial electrojet, *J. Geophys. Res.*, *117*, A03306, doi:10.1029/2011JA017351.

Pedatella, N. M., and H.-L. Liu (2013), The influence of atmospheric tide and planetary wave variability during sudden stratosphere warmings on the low latitude ionosphere, *J. Geophys. Res. Space Physics*, *118*, 5333–5347, doi:10.1002/jgra.50492.

Rastogi, R. G., and J. A. Klobuchar (1990), Ionospheric electron content within the equatorial F2 layer anomaly belt, *J. Geophys. Res.*, *95*, 19,045–19,052, doi:10.1029/JA095iA11p19045.

Scherhag, R. (1952), Die explosionsartigen Stratosphärenerwärmungen des Spätwinters 1952, *Ber. Dtsch. Wetterdienstes US Zone*, *6*, 51–63.

Erratum

In the originally published version of this article, several instances of text were incorrectly typeset. The following have since been corrected and this version may be considered the authoritative version of record.

In Section 2, +20° was changed to ± 20°.
In Section 4, +20° was changed to ± 20°.